Computational Modeling of Laminated Veneer Bamboo Dowel Connections

Niloufar Khoshbakht[1]; Peggi L. Clouston, M.ASCE[2]; Sanjay R. Arwade[3]; and Alexander C. Schreyer[4]

Abstract: Laminated veneer bamboo (LVB) is a relatively new building product made from layers of glued bamboo and used in applications similar to lumber. Few studies exist on its mechanical performance; in particular, its failure behavior in dowel-type connections. This study uses both experimental and numerical methods to shed light on the complex stress state of an LVB dowel connection when progressively loaded in compression parallel to grain. A 2D elastic, plane strain finite element model is developed for a 15.9-mm (5/8-in.)-diameter bolt with a bolt hole size of 17.5 mm (11/16 in.) following the associated ASTM standard for full-hole specimen protocol. Experimental tests are used to validate and calibrate the model. Results show that predominant failure occurs off-center of the bolt contact region where the shear stress-to-strength ratio governs. Tensile stress perpendicular to grain, often the primary cause of wood failure, is found to be an influential secondary cause of failure. In addition, a frictional contact analysis leads to the finding that the coefficient of friction is a key factor in predicting shear stress. **DOI: 10.1061/(ASCE)MT.1943-5533.0002135.**

Author keywords: Moso bamboo; Composite; Dowel connection; Embedment strength; Failure behavior; Finite element analysis.

Introduction

Bamboo is a fast-growing plant that has been used in construction for centuries in many parts of the world where it is naturally grown (Lee et al. 1994). Its sustainable attributes are well known: for example, its maturation cycle for harvest is a mere 3–8 years (Mahdavi et al. 2011), its rate of carbon sequestration is more efficient than any wood species, and its processing is low energy intensive and creates minimal pollution (Diesen and Clouston 2014). Consequently, bamboo is becoming an attractive material in regions of the world where it is not native.

Although the natural cylindrical form of the bamboo culm is inherently strong, it is not overly practical, particularly in consideration of structural connections. Laminated veneer bamboo (LVB), however, is a composite material made from bamboo that possesses bamboo's desirable mechanical properties but has the added benefit of being prismatic, being produced in stock sizes, and allowing for standard connection hardware, similar to engineered wood products (Mahdavi et al. 2011). Although LVB is currently commercially available and sold worldwide, fundamental research is still needed to fully define and understand the aspects of connection failure, such as its tendency to split under dowel-bearing loads (Diesen and Clouston 2014). Ultimately, the hope is that this type of research will lead to improvements in bamboo connection detailing and design to facilitate worldwide adoption of bamboo in modern construction.

Most previous studies on dowel bearing capacity have naturally been conducted on softwood lumber species, whereas only a small number of studies have been carried out on laminated bamboo connections. This study aims to progress from this body of knowledge by starting with understanding how or if LVB dowel connection behavior differs from that of timber for design codes and standards development.

The national design specification (NDS) for Wood Construction (AWC 2015) uses a reference design value (Z) representing the basic capacity of a dowel fastener under short-term lateral load where the yielding of various elements in the connection contributes to failure. The Z term derives from the European yield model (EYM) originally proposed by Johansen (1949) and is widely used for design of laterally loaded fasteners. The EYM considers the connection geometry and wood and fastener material properties to evaluate strength while assuming the wood to be a rigid plastic material. According to Johansen's yield model (CEN 2007), the embedment strength is expressed as the maximum applied load divided by the contact area [Eq. (1)]

$$f_h = \frac{F_{\max}}{t * d}\left[\frac{\mathrm{N}}{\mathrm{mm}^2}\right] \tag{1}$$

Based on the EYM, the embedment strength is most influential for a Mode I failure strength (Soltis 1991), whereby wood crushing is the main mode of failure. Wood crushing failure occurs around the bolt hole because of high stress concentrations in this area (Oudjene and Khelifa 2009). Although the EYM estimates a design strength and corresponding failure mechanism, it does not provide an understanding of the complex stress state in the material beneath the contact surface. Because of the cellular and porous characteristics of wood (and presumably bamboo), the problem is geometrically and materially nonlinear and demands more investigation.

The most predominant failure modes of the wood in the connection were reported to be initiated by shear and tension perpendicular-to-grain stresses (Branco et al. 2009). Shear pull-out

[1]Graduate Student, Dept. of Environmental Conservation, Univ. of Massachusetts, Amherst, MA 01003 (corresponding author). ORCID: https://orcid.org/0000-0003-3825-1334. E-mail: nkhoshbakht@umass.edu

[2]Associate Professor, Dept. of Environmental Conservation, Univ. of Massachusetts, Amherst, MA 01003. E-mail: clouston@umass.edu

[3]Associate Professor, Dept. of Civil and Environmental Engineering, Univ. of Massachusetts, Amherst, MA 01003. E-mail: arwade@umass.edu

[4]Lecturer, Dept. of Environmental Conservation, Univ. of Massachusetts, Amherst, MA 01003. E-mail: mail@alexschreyer.net

Note. This manuscript was submitted on December 12, 2016; approved on July 13, 2017; published online on December 8, 2017. Discussion period open until May 8, 2018; separate discussions must be submitted for individual papers. This paper is part of the ***Journal of Materials in Civil Engineering***, © ASCE, ISSN 0899-1561.

(a.k.a. plug shear failure), which is caused by combined shear and tensile perpendicular-to-grain stresses along the outer edge of the dowel–wood contact zone, was noted as a related failure mode. In terms of loading direction, compressive loading in the parallel-to-grain direction was reported to be the cause of brittle failure in wood connections (Kharouf et al. 2003).

The embedment strength of a wood dowel connection depends on geometric parameters, such as hole diameter and hole end distance, as well as material properties. Santos et al. (2010) investigated the embedment strength of a dowel-type connection with maritime pine loading in the longitudinal and tangential directions. Shear splitting was observed in the longitudinal-tangential plane when loading parallel to the grain, whereas low tension strength seems to be responsible for failure when loading perpendicular to the grain direction. However, the predicted values of failure from the FE model were lower than the experimental values.

Bamboo products are sometimes assumed to behave like hardwood material (Dixon and Gibson 2014). Although many studies and formulations involving bearing strength are derived from softwood species, a handful of studies have focused on hardwood. For example, a 2007 study was conducted on the tropical hardwood Shorea obtuse (Awaludin et al. 2007) to find dowel-bearing properties for several test configurations, and the results were compared with formulations from NDS and Eurocode 5 standards (CEN 2005). The authors found that the estimated bearing strengths using equations from the NDS were higher than those of their experiments and other empirical equations. Moreover, no previous studies or standards on loading perpendicular to the grain were capable of properly predicting failure, testifying to the fact that more research is needed in this area.

Patton-Mallory et al. (1997) focused on bolted connections loaded parallel to grain. The authors used a trilinear stress-strain relationship to predict the strength behavior of the bolted connections. When loaded parallel to grain, the prediction of the connection failure showed good conformity with experimental results for loading up to 0.762 mm displacement. However, it was noted that the model was not sensitive to small changes in material properties and thus shows the same failure mode prediction.

A few studies have been published on failure analysis of bamboo-laminated products. Yang et al. (2014) performed failure analysis of Glubam, an engineered bamboo material that is assumed bidirectional in terms of fiber direction. The authors revised the Hankinson formula so that it could explain the material behavior at different fiber angles based on an off-axis tension test. Further, they worked on finding Tsai-Wu parameters, specifically, the interaction parameter F_{12} at an angle of 15°. Based on the experimental data, the Tsai-Wu failure criterion was unable to explain the failure behavior of Glubam.

Work was done by Ramirez et al. (2012) on laminated Guadua bamboo dowel joints to experimentally determine the effect of different hole diameters and loading directions on bearing strength. The authors found a meaningful relation between bearing strength and fastener geometry, including diameter and width-to-diameter ratio. They also developed a FE model based on their experimental results and determined an experimental formula to explain the local behavior of the loading zone around the bolt hole as a function of bulk material properties. However, in the finite elements (FEM) results, failure mechanism and failure mode were not discussed.

Recent work by Reynolds et al. (2016) revealed a meaningful difference in failure mechanism between Moso bamboo dowel joints and timber dowel joints. Based on digital imaging experiments and full-field strain measurements, it was deduced that high shear stresses around the bolt hole are responsible for bamboo dowel failure, whereas failure in timber joints is attributed to tensile strain perpendicular to the grain. The authors used a numerical model based on the Lekhnitskii stress function (Lekhnitskiĭ 1968) and explained that the different failure behaviors of laminated bamboo products are because of coefficient of friction and orthotropic material property differences between timber and engineered bamboo.

The EYM presents an effective design method for timber dowel connections, but it remains to be seen whether the assumptions for wood can be made for LVB dowel connections. The objective of this study is thus to elucidate LVB dowel failure mechanisms in compression loading parallel to grain and to further understand LVB dowel connection behavior for design codes and standards development.

Experimental Program

LVB Material Property Tests

The material properties of LVB: shear, tension and compression strengths parallel and perpendicular to grain, were experimentally determined and applied as input parameters for subsequent FEM studies of the dowel joints. In the experimental tests, commercially available LVB boards were used made from Moso bamboo (*Phyllostachys heterocycla var. pubescens*). The LVB was purchased from the Lamboo company and consists of $1/4 \times 3/4$-in. bamboo culm slats that are bonded together with ANSI/HPVA Type 1 adhesive.

The boards were conditioned for a minimum of 2 months in constant ambient environmental conditions. The mean moisture content of the samples was 5.4% (COV 5%) as measured by the oven dry method [ASTM D2016 (ASTM 1991)].

Compression Tests

To evaluate compression strength and elastic properties, 10 specimens (calculated based on ASTM D2915 (ASTM 1999) with a confidence level of 99%) were machined from $3{,}000 \times 150 \times 35$ mm LVB boards for each sample. For the parallel-to-grain loading direction, specimen dimensions were $25 \times 25 \times 100$ mm, whereas $50 \times 50 \times 150$-mm specimens [ASTM D143 (ASTM 1994)] were used for the perpendicular-to-grain direction.

Loading was applied continuously at a rate of 0.012 in. (0.305 mm/min) using a 150 kN material testing system (MTS) machine. The displacement was measured using a uniaxial extensometer (MTS634.11F-24) for the parallel-to-grain compression test (Fig. 1) and a linear variable displacement transducer (LVDT) for the perpendicular-to-grain test (Fig. 2).

Tension Tests

Samples were prepared in accordance with ASTM D3500 (ASTM 2009) for small tension specimens of structural panels. The samples were cut from $300 \times 150 \times 35$-mm LVB boards with a CNC machine to ensure that the exact profile and dimensions were achieved. Tension loading was applied according to ASTM D3500 so that failure occurred within 3–10 min [Fig. 3(b)]. Ten specimens were tested, and Table 1 displays the material property values with corresponding loading directions. The load-displacement curve in Fig. 3(c) confirms the expectation that LVB in tension follows a linear, brittle failure behavior.

The tension test for the perpendicular-to-grain direction was performed on 10 specimens in accordance with ASTM D143 at the same loading speed (0.305 mm/min) (Fig. 4). The results are provided in Table 1.

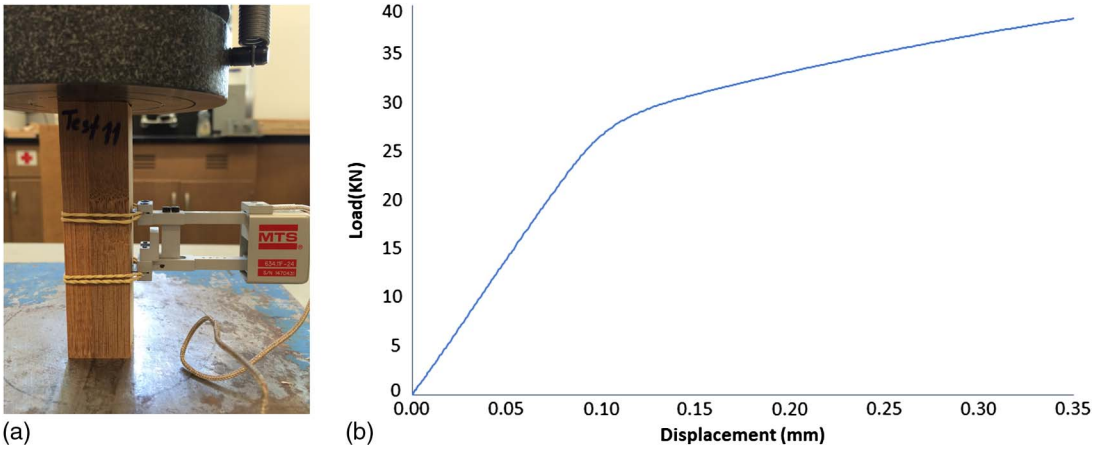

Fig. 1. (a) Compression test setup parallel to grain; (b) typical load-displacement curve

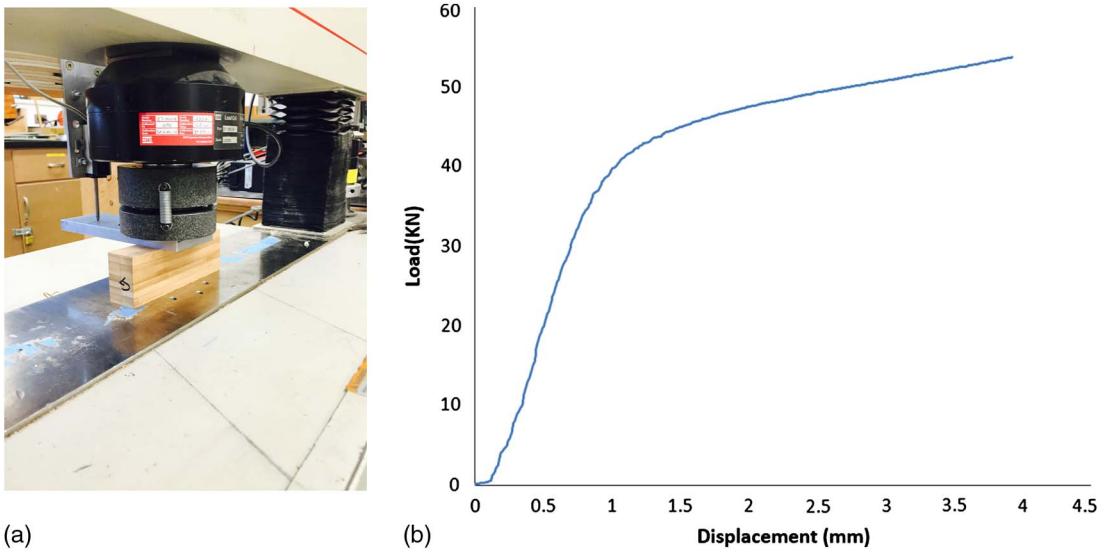

Fig. 2. (a) Compression test setup for perpendicular-to-grain direction; (b) typical load-displacement curve

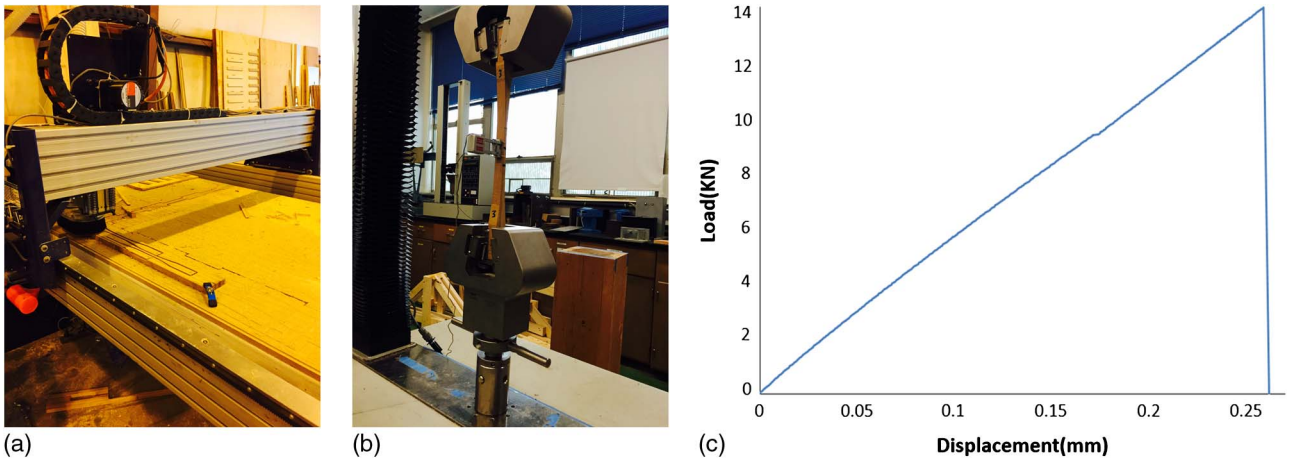

Fig. 3. Tension test: (a) fabrication; (b) test setup; (c) typical load-displacement curve

Table 1. Material Properties of Moso Laminated Veneer Bamboo

Loading direction	Density (kg/m^3)	Compression MOE (MPa)	Compression Strength (MPa)	Tension MOE (MPa)	Tension Strength (MPa)	Shear Strength (MPa)
Parallel	650	11,600	62	9,219	95	13.15
COV (%)	—	7	3.2	15	12	11
Perpendicular	650	1,440	28	200	5.43	—
COV (%)	—	30	11	9	22	—

Note: COV = coefficient of variation.

Shear Tests

The shear test was performed according to ASTM D143 and at a loading rate of 0.6 mm/min. Fig. 5 shows the test equipment and the shear block subjected to continuous loading. According to the standards, the shear area was 50.8 × 50.8 mm (2 × 2 in.) and the average shear strength was found to be 13.15 MPa. No glue failure was observed in the sample.

LVB Embedment Properties

Test Setup

The material preparation and test procedure for evaluation of embedment properties followed ASTM D5764 (ASTM 2013) for a single dowel joint using wood-based products (Figs. 6 and 7). The sample consisted of 15 replications as determined by ASTM D2915. An MTS3000 testing machine was used in combination with an LVDT and extensometer to measure displacement both at the contact surface and beneath the contact area of a single dowel joint.

ASTM D5764 guidelines recommend using full-hole specimens instead of half-hole specimens for specimens that tend to split before the completion of the test. Therefore, to provide a more realistic measurement of dowel joint behavior, full-hole specimens were used.

The LVB specimens measured 152 × 63 × 32 mm^3. The hole was bored with a 17.5-mm (11/16-in.)-diameter drill bit to accommodate a 15.9-mm (5/8-in.)-diameter steel (grade 5.5) bolt. The steel

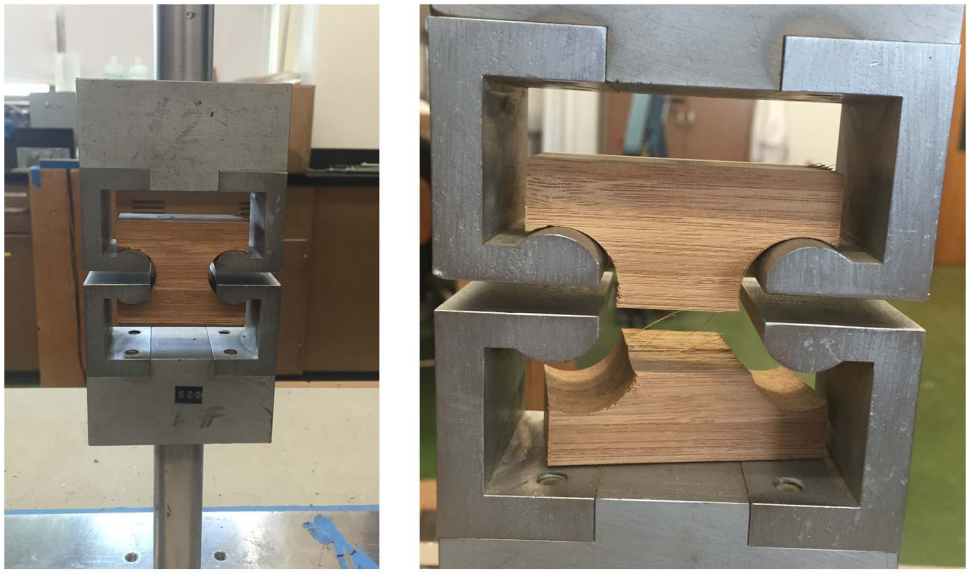

(a) (b)

Fig. 4. Tension test: (a) setup perpendicular to grain; (b) failure due to loading perpendicular to grain

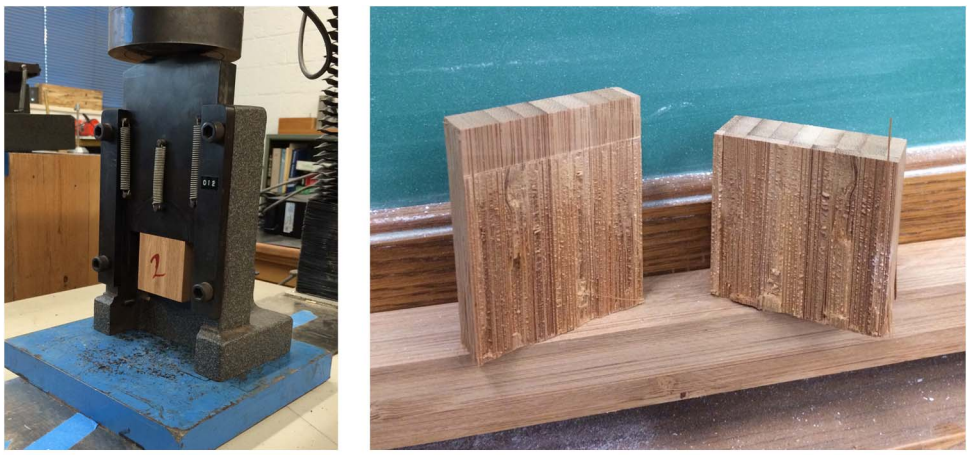

(a) (b)

Fig. 5. Shear test: (a) test setup; (b) specimen shear failure surface

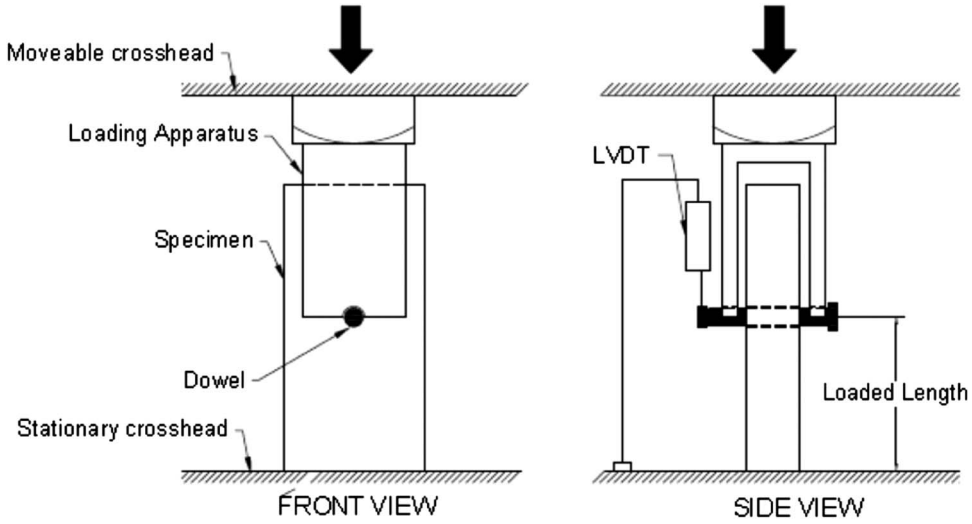

Fig. 6. Embedment test setup based on ASTM D5764 (adapted from ASTM D5764)

loading apparatus was fabricated to ensure application of the load onto the wood contact surface was imparted directly through the smooth surface of the steel bolt. A crosshead rate of 1 mm/min produced failure within 1–10 min. Displacement directly beneath the contact zone was obtained by means of a LVDT (Fig. 7). An MTS634.11F-24 extensometer was also used to observe the material strain at a 25 mm distance beneath the midpoint of the contact surface.

Test Results

Table 2 shows the stiffness values (N/mm) at the contact surface and beneath the contact surface (extensometer zone). The results indicate that the material stiffness at the contact surface is 10.6 times less than the stiffness measured in the extensometer zone. In view of this result, two definitions for material elasticity are used for the subsequent stress analysis in this paper: bulk modulus of elasticity and local modulus of elasticity at the contact surface.

Fig. 8 displays a failure pattern of the dowel joint after loaded parallel to grain until it reached its maximum strength within 0.9–1.2 mm LVDT displacement. In 80% of the specimens, the crack started and continued to grow at between 4 and 4.7 mm off center (i.e., 1/6 of the hole perimeter left or right of center) beneath

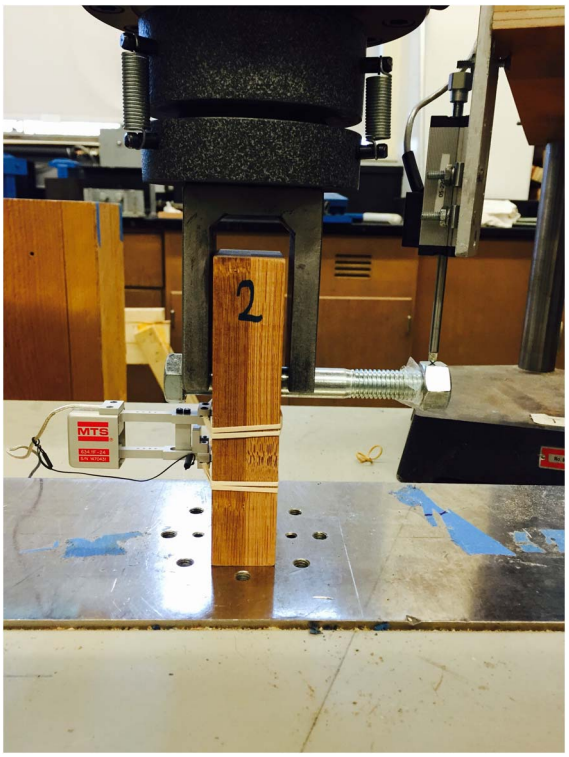

Fig. 7. Embedment test setup: displacement was measured in contact zone (LVDT) and beneath the contact zone (extensometer)

Table 2. Stiffness Measured at Contact Surface and beneath the Contact Surface

Parameter	Stiffness in extensometer zone (N/mm)	Stiffness at contact surface (N/mm)	Embedment strength parallel-to-grain (MPa)
Mean	343,600	32,400	49
COV (%)	14.4	5.6	8

Note: COV = coefficient of variation.

Fig. 8. Splitting failure in LVB dowel joint when loaded parallel to grain

the loaded area. Another split occurred on the top of the bolt hole during the last stage of loading as a result of plane separation in the bottom section. It is important to note that no glue failure was observed. These tests suggest that a combination of tension perpendicular to grain and shear stresses on the specimen is responsible for failure.

Finite Element Model

In order to investigate the stress distribution at and beneath the contact surface, a 2D plane strain FE model was developed using *ADINA* software. The model geometry was the same as the experimental full-hole test setup described in ASTM D5764. Fixed displacement was assumed at all bottom nodes and compressive load was applied to the bolt in the form of displacement. The effect of a 1.6 mm (1/16-in.) larger bolt hole to bolt diameter (tolerance per NDS) was also considered in the model.

A contact surface was defined between the steel bolt and the LVB hole. The bolt was assumed to be a rigid body under a condition that is called a rigid-target contact problem often used for cases when the two bodies have substantially different material stiffness (e.g., $E_1 = 10^{10}E_2$) (Frastia 2007). According to Kim (2015), the stiffness matrix becomes ill conditioned when the stiffer body of the two is not assumed rigid, which leads to uncertainty in the accuracy of the solution.

Incremental loading steps of a 0.001-mm displacement were applied, to start, by controlling the time function value. After validation of the results, the applied displacement was increased to 1 mm by changing the time points gradually until the LVB dowel joint reached its maximum strength according to the load-displacement curve.

Material Property Assumptions

The Moso LVB was modeled as linear elastic, orthotropic material with constitutive properties from Table 1. Values for the less influential parameters, Poisson ratio and shear modulus, were selected from the literature: the former value being between 0.22 and 0.25 as noted by Yu et al. (2011) and the latter value being 745 MPa as reported for Moso bamboo (Askarinejad et al. 2015).

The material axes directions (Fig. 9) were modeled to coincide with the global axes directions (*ADINA*). To ensure that the stiffness and compliance matrices were positive definite, in order to reach a solution, the material property input values complied with *ADINA* nomenclature for Poisson ratio per Eq. (2) (*ADINA*), which differs from the general notation (Jones 1999) of Poisson's ratio [Eq. (3)]

$$\frac{\vartheta_{ij}}{E_j} = \frac{\vartheta_{ji}}{E_i} \quad i, j = a, b, c \tag{2}$$

$$\vartheta_{ij(ADINA)} = \left(\frac{E_j}{E_i}\right)\vartheta_{ij(Jones)} \quad i, j = a, b, c \tag{3}$$

Element Selection

A 2D plane strain model was developed with both eight-node and nine-node quadrilateral elements (Q8 and Q9). Mesh refinement was performed in the area of interest around the bolt hole (Fig. 9). Both Q8 and Q9 elements converged to the same solution results. Based on this convergence study, Q9 with side lengths of 0.5 mm at the area of interest was chosen.

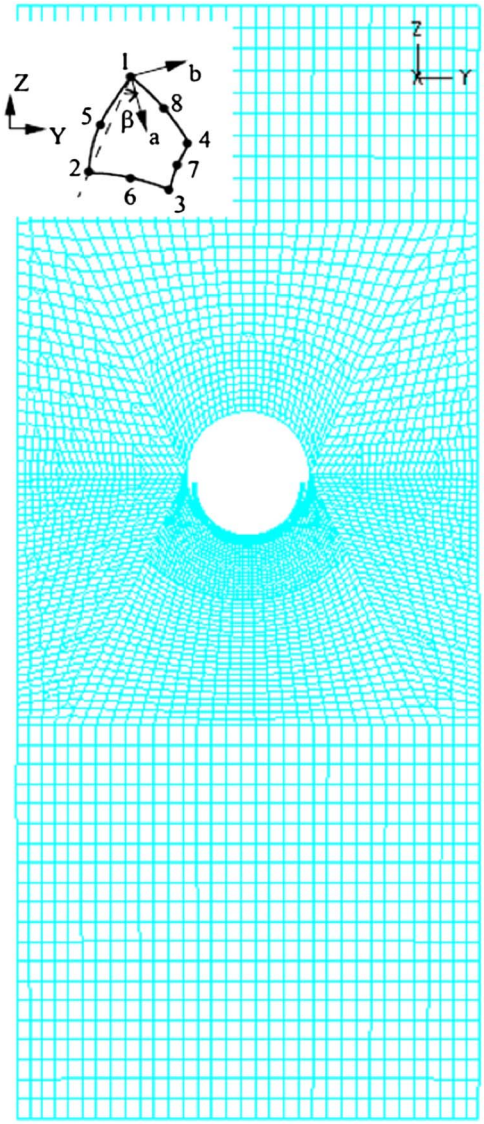

Fig. 9. FEM element local and global coordinates and mesh

Model Calibration

It was found that several important parameters affect the FE model contact behavior. They are explained in detail subsequently:

- Contact stiffness: This value is defined as a penalty parameter that is based on the material stiffness and contact element size. A larger value allows for less penetration but may lead to difficulties in convergence. In *ADINA*, contact stiffness is defined by a scale factor known as the compliance factor, which is usually assumed to be a value of 0.001. The *ADINA* software manual suggests a penetration value on the order of 1% of the element size (*ADINA*). Thus, the compliance factor is chosen so that it allows appropriate penetration;
- Mesh at contact area: The relative mesh size of the contact or target surface was selected to avoid penetration of the contact body into the target body (Kim 2015) by making certain that the target body had a coarser mesh than the contact surface [Fig. 10(a)]. Usually, the flat or stiffer body is selected as the target to decrease penetration and minimize numerical error.

Moreover, the element size should be tested in the most probable contact zone so that the normals of the contact and target surfaces interact properly with each other. Because of the C0

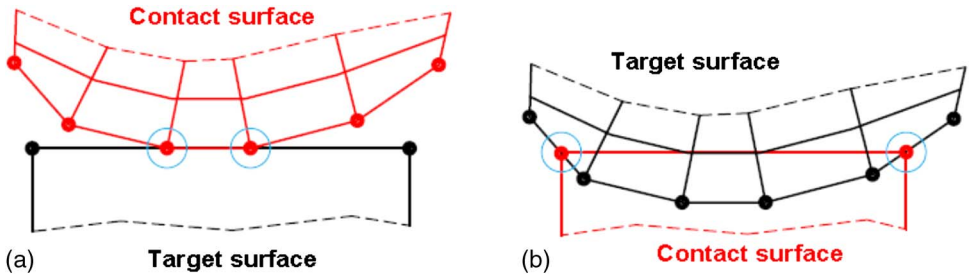

Fig. 10. Contact area mesh model effect on penetration: (a) target surface with coarser mesh; (b) contact body with coarser mesh

Table 3. FEM Calibration in Compressive Loading Parallel to the Grain

Model				Results			
FEM model	Mesh size (mm)	Compliance factor	Displacement (mm)	U_Z (mm)	Contact force on contact line [F_Z (N/mm)]	Contact pressure (MPa)	Contact stiffness [K (N/mm)]
1	0.5	0.0001	1	0.96	1,257	37,760	37,760
2	0.5	0.0002	1	0.93	1,140	36,480	36,480
3	0.5	0.0003	1	0.9	1,170	35,200	35,200
4	0.5	0.0004	1	0.87	1,070	34,240	34,240

continuity across the contact boundary, the contact force is very sensitive to mesh discretization. It was found that the results change abruptly with mesh refinement, so careful consideration should be placed on mesh refinement at the contact boundary; and

- Contact tolerance: This value is the minimum distance that the program searches for contact and calculates contact force with lower computer cost. The contact tolerance is usually 1% of the contact element length (Kim 2015). It is important because choosing proper contact tolerance, together with proper load increment, leads to converged and more accurate results.

In both Lagrange multiplier and penalty methods, the contact is treated as a constraint (Kim 2015) in the structural equilibrium, which is why the contact formulation is independent of the material constitutive models.

By considering all of the previous, the model was calibrated to experimental results by using different combinations of mesh size, contact stiffness, load increments, and contact tolerance. Table 3 presents the FE model stiffness results assuming a value of 0.2 for coefficient of friction between LVB and steel dowel (Reynolds et al. 2016). Ideally, the displacement in the contact zone (U_Z) should be equal to the applied displacement on the rigid bolt, which should lead to zero penetration; however, in practice, for choosing a realistic model, there should be a compromise between penetration and contact stiffness. Accordingly, the optimal FE model (No. 4) was chosen based on Table 3, which has a reasonable U_Z and the closest stiffness to that of the experimental results. The value for K from the FE model No. 4 is 34,240 N/mm, which is the closest to the K mean value (32,400 N/mm, COV 5%) from the embedment tests.

Local Elastic Moduli Evaluation

The localized moduli of elasticity (E_L) [as opposed to the bulk modulus of elasticity (E_B)] is necessary as input to the FE model. Two distinct values for E_L were considered: parallel to grain and perpendicular to grain to account for the significant orthotropicity of the material (i.e., E parallel $\gg$ E perpendicular). Also, the splitting failure in LVB is in large part because of tensile stresses perpendicular to grain, and the respective E values play an important role in the accuracy of the model.

The local elastic modulus (E_L) parallel to grain was determined following an empirical approach. The method is based on embedment test data and Eq. (4), derived from Hooke's law, where K is the mean slope of the linear portion of the load-displacement curves slope of the embedment test

$$E_L = K * \frac{L}{A} \tag{4}$$

where K = slope (N/mm); A = bolt projected area (mm^2); and L = bearing zone depth (mm).

According to Hong et al. (2011), the most important parameter that affects the bearing zone depth L is the dowel geometry. The depth of the bearing zone for their calculations was assumed to be equal to the dowel diameter D. Later, Ramirez et al. (2012) based on experimenting with varying dowel diameters in their FEM model for Guadua bamboo, suggested the simple equality that $L = 1.6D$. Following the same path, according to the present FEM model, the bearing zone depth was found to be $1.4D$ for Moso LVB.

Based on calculated bearing depth, the E_L parallel-to-grain value used in the stress analysis was considered to be 1,007 MPa (COV 15%) from Eq. (4).

The local elastic modulus (E_L) perpendicular to grain was calculated from the tension perpendicular-to-grain test data where K was found from the mean slope of the linear portion of the load-displacement curves. The E_L perpendicular-to-grain mean value used in the stress analysis was calculated to be 200 MPa. The results are summarized in Table 4.

Finite Element Analysis

The calibrated FE model was used to examine the stress state of Moso LVB in the zone under the dowel, the purpose being to gain insight into the progressive nature and exact cause of failure. The investigation focused on the progression of key individual stresses as displacement was increased to near failure. 1 mm was the upper

Table 4. Finding Local Modulus of Elasticity Based on Embedment and Tension Test Results

Test	Sample size	Failure load (N)	Failure displacement (mm)	Local modulus of elasticity (MPa)
Parallel-to-grain (embedment test)	15	—	—	—
Mean value	—	28,197	1.18	1,007
COV (%)	—	8	15	15
Perpendicular-to-grain (tension test)	10	—	—	—
Mean value	—	4,450	0.55	200
COV (%)	—	22	19	9

Note: COV = coefficient of variation.

limit chosen because the experimental embedment tests indicated that failure occurred, on average, at 1.18 mm (COV 15%).

Fig. 11 illustrates the magnitude of compressive stress in the z- (parallel-to-grain) direction as it decreases with vertical distance from the center point of the hole at three stages of incremental displacement: 0.1, 0.5, and 1 mm. For this stress, the stress-distance curve for each load increment follows a similar trend; this is not so for other stresses, as will be shown. At 1 mm displacement, the maximum elemental stress in the z-direction is less than mean strength per Table 1 (56 < 62 MPa), suggesting that, though certainly an influence on incipient failure in that zone, σ_{zz} is not the primary cause.

Figs. 12 and 13 depict stress contours around the bolt hole at high levels of load for tensile stress perpendicular to grain (σ_{yy}) and in-plane shear stress (σ_{yz}), respectively. Notably, the stress levels shown exceed strength values given in Table 1 for both stresses, indicating that failure (at least at the elemental level) has already occurred. The locations of highest stress for both stresses match closely with the visual results for splitting failure that were observed in the experimental tests except for the contact edges of steel bolt and LVB material. In Fig. 13, the model predicted that the dowel joint begins to fail at approximately 0.95 mm of applied displacement, 18% off from the experimental mean value (1.18 mm).

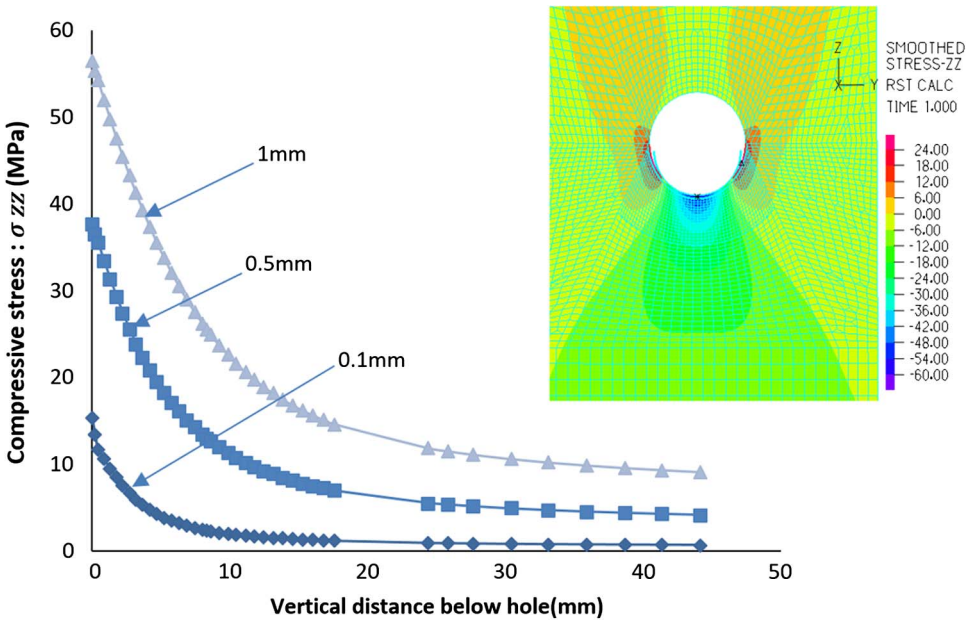

Fig. 11. Parallel-to-grain compressive stress distribution below hole for three displacements

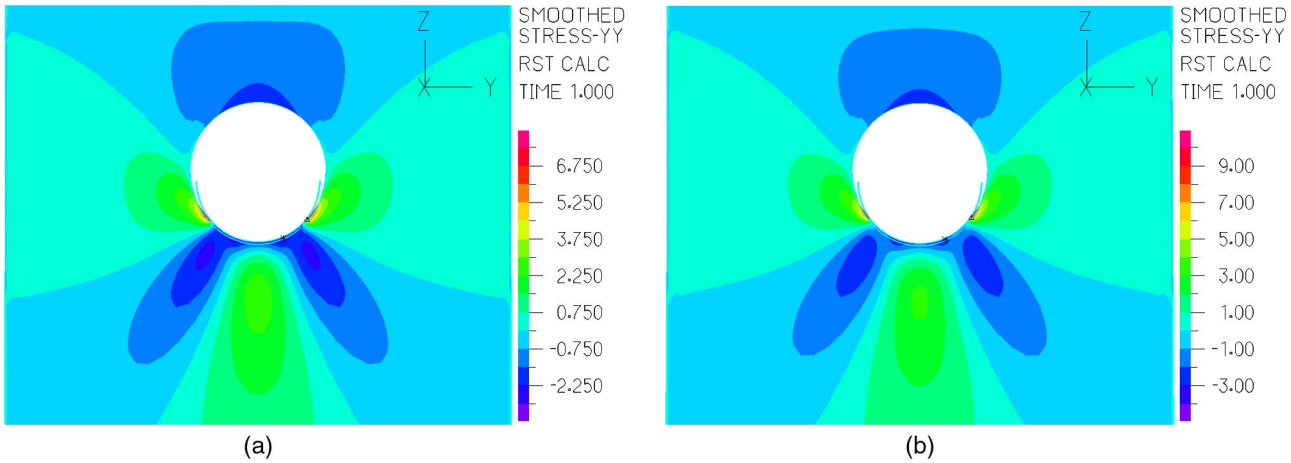

Fig. 12. Perpendicular-to-grain tensile stress contours with (a) 0.8 mm displacement; (b) 1 mm displacement

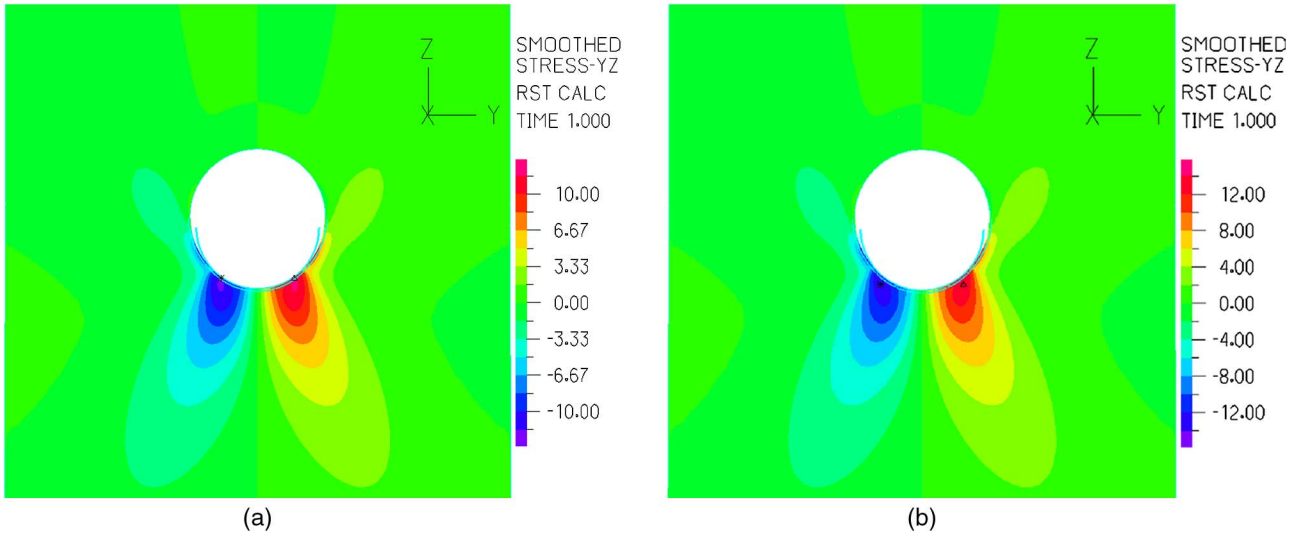

Fig. 13. In-plane shear stress contours with (a) 0.8 mm displacement; (b) 0.95 mm displacement

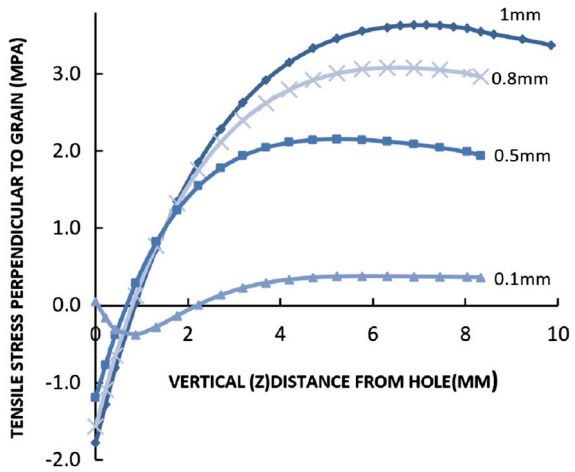

Fig. 14. Perpendicular-to-grain tensile stress distribution on plane below contact surface for four displacements

Figs. 14 and 15 illustrate how tensile stress perpendicular to grain varies with vertical and horizontal distance from the center point of the hole at four stages of incremental displacement. According to the data points selected in the vertical distance from the contact surface in Fig. 14, the maximum tensile stress occurs at 7.4 mm underneath the contact surface. Fig. 14 indicates that as the loading increases, the stress distribution changes because of the change in the contact surface area. Also, as the loading increases, the contact surface enters the stage of slip contact (Fig. 16). The maximum tensile stress is 3.6 MPa at 1 mm displacement (roughly failure), which is slightly less than 5.4 MPa (experimental LVB strength in Table 1). However, the coefficient of variation for strength from the embedment test results (22%) would suggest that tension stress perpendicular to grain clearly also contributes to the cause of failure.

Fig. 17 illustrates how the location of the maximum shear stress changes as the loading increases and also shows how the maximum shear stress is affected by friction. Because there are only normal contact forces in the contact region, the maximum shear stress

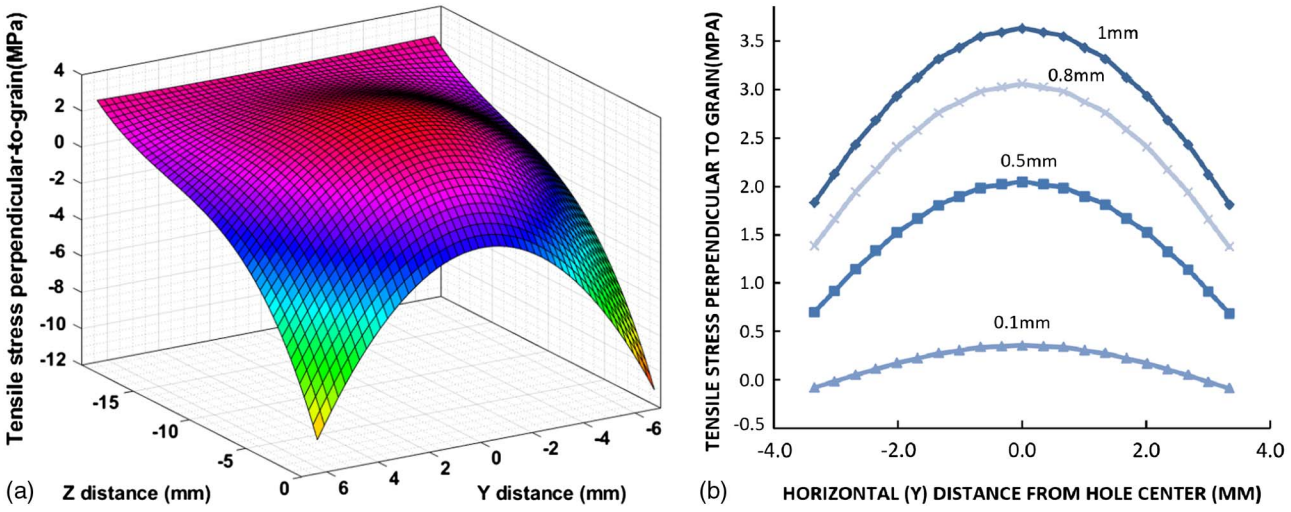

Fig. 15. Perpendicular-to-grain tensile stress distribution: (a) in 3D space; (b) across horizontal plane at 7.4 mm below hole for four displacements

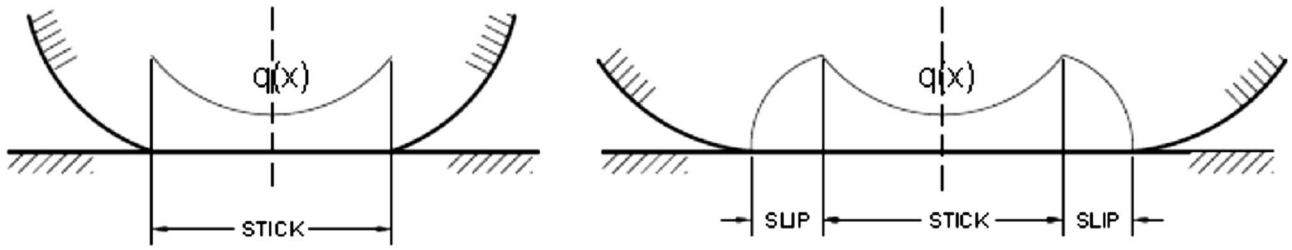

Fig. 16. As the vertical loading increases, the contact surface enters the slip region

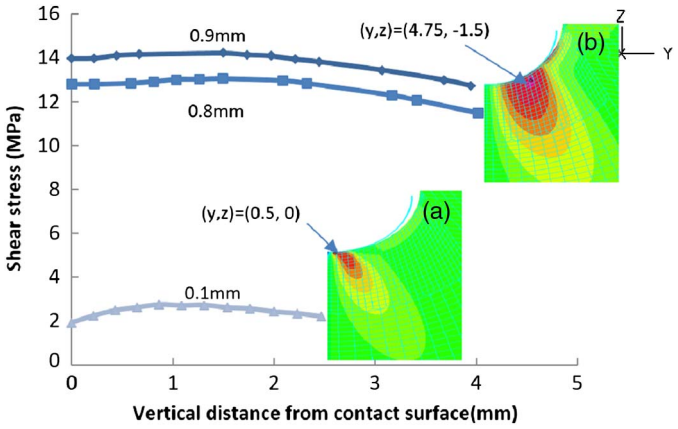

Fig. 17. Shear stress values on vertical distance from the contact surface and shear stress contours: (a) surface stress field in sticking contact; (b) the location of maximum shear stress moves outward because of sliding contact

is very close to the contact center when a 0.1-mm load increment is applied [Fig. 17(a)]. When the load increases, the contact surface enlarges (Fig. 16) and tangential forces appear. In this case, the stress pattern is also affected by slip and frictional forces [Fig. 17(b)], which cause the location of maximum shear stress to move outward and away from the contact surface. Given this stress state, the FE model predicts the location of the maximum shear stress at 4.75 mm horizontally off center, which is confirmed by the embedment experiment results. For 80% of the sample size (reference Fig. 8), the fracture initiated between 4 and 4.7 mm off center (lower 1/6 of the hole perimeter), and the other 20% displayed a fracture on center.

As depicted in Fig. 17(b), the maximum shear stress occurs at 1 mm beneath the contact zone. This is consistent with the experimental observations in which the fracture starts underneath the surface and develops up to the surface as the loading increases.

Conclusions

The purpose of this study was to investigate the embedment response of LVB when loaded by a steel dowel in compression parallel to grain. To that end, a series of experimental tests were conducted to measure tension, compression, and shear properties of LVB, which were further used as input into the finite element model. Full-hole tests were conducted in accordance with ASTM D5764 for a 15.9-mm (5/8-in.) diameter bolt with a slightly larger bolt hole size of 17.5 mm (11/16 in.) as per the hole tolerance practices outline in the NDS for wood construction. The finite element model was built to simulate this test, calibrated to match experimental results, and then used to inspect stress distributions at various levels of displacement in the critical zone under the bolt. The model was novel in that it included contact elements assuming a rigid-target contact problem between the bolt and the LVB, leading to new information about frictional effects.

The key findings of the study were as follows:

- In calibrating the finite element model, it was found necessary to define a functional local modulus of elasticity (E_L) to be used in place of bulk modulus (E_B), the two values differing by a factor of approximately 10.2 (1,140 versus 11,600 MPa). This calibration approach is consistent with that conducted in a previous study on Guadua Bamboo by Ramirez et al. (2012);
- The FE model predicted that the LVB dowel joint begins to fail at approximately 0.95 mm of applied displacement, matching experimental results within reasonable limits of statistical variability;
- Both the experimental and FEM results indicate that in-plane shear stress was the primary cause of LVB failure through concurring measures of both failure load and location. Failure typically occurred off hole center, at 1/6 of the hole perimeter left or right of center, which according to the FEM is in the high shear stress zone where tension perpendicular-to-grain stresses were moderate. The model further elucidates that with each load increment, the location of maximum shear stress moves further outward from the hole center and further underneath the contact surface;
- Tension perpendicular-to-grain stresses were shown to be a secondary contributing factor to failure. Maximum tensile stress occurred 7.4 mm beneath the hole, at the center of the contact region, with an increasingly heightened distribution as applied displacement increased; and
- The FE model showed high sensitivity to frictional forces, indicating that they play an important role in how the model predicts the location of maximum shear stresses. It is suggested that future studies delve further into this area of how the coefficient of friction between the steel bolt and LVB material influences LVB failure.

Acknowledgments

This material is based upon work that is supported by the National Institute of Food and Agriculture, U.S. Department of Agriculture, MAS00026/1000963. The authors would like to thank Dan Pepin, shop manager of the Building and Construction Technology program at the University of Massachusetts, for his contributions to the project.

References

ADINA system 9.2 [Computer software]. ADINA R&D, Inc., Watertown, MA.

Askarinejad, S., Kotowski, P., Shalchy, F., and Rahbar, N. (2015). "Effects of humidity on shear behavior of bamboo." *Theor. Appl. Mech. Lett.*, 5(6), 236–243.
ASTM. (1991). "Standard test methods for moisture content of wood." *ASTM D2016*, Philadelphia.
ASTM. (1994). "Standard methods of testing small clear specimens of timber." *ASTM D143*. Philadelphia.
ASTM. (1999). "Standard practice for evaluating allowable properties for grades of structural lumber." *ASTM D2915*, Philadelphia.
ASTM. (2009). "Standard test methods for structural panels in tension." *ASTM 3500D*, Philadelphia.
ASTM. (2013). "Standard test method for evaluating dowel-bearing strength of wood and wood-based products." *ASTM D5764-97*, Philadelphia.
Awaludin, A., Smittakorn, W., Hirai, T., and Hayashikawa, T. (2007). "Bearing properties of Shorea obtusa beneath a laterally loaded bolt." *J. Wood Sci.*, 53(3), 204–210.
AWC (American Wood Council). (2015). *NDS, national design specification for wood construction*, Leesburg, VA.
Branco, J., Cruz, J., and Piazza, M. (2009). "Experimental analysis of laterally loaded nailed timber-to-concrete connections." *Constr. Build. Mater.*, 23(1), 400–410.
CEN (European Committee for Standardization). (2005). "Design of timber structures. Part 1-1: General rules and rules for buildings." *Eurocode 5, EN 1995-1-2*, Brussels, Belgium.
CEN (European Committee for Standardization). (2007). "Timber structures. Test methods. Determination of embedding strength and foundation values for dowel type fasteners." *EN 383*, Brussels, Belgium.
Diesen, K., and Clouston, P. (2014). "Building with bamboo: A review of Culm connection technology." *J. Green Build.*, 8(4), 83–93.
Dixon, P., and Gibson, L. (2014). "The structure and mechanics of Moso bamboo material." *J. R. Soc. Interface*, 11(99), 20140321.
Frastia, L. (2007). "Numerical solution of elastic bodies in contact by FEM utilizing equilibrium displacement fields." *Comput. Mech.*, 41(1), 159–174.
Hong, J. P., Barrett, J. D., and Lam, F. (2011). "Three-dimensional finite element analysis of the Japanese traditional post-and-beam connection." *J. Wood Sci.*, 57(2), 119–125.
Johansen, K. W. (1949). "Theory of timber connections." *Int. Assoc. Bridge Struct. Eng.*, 9, 249–262.
Jones, R. (1999). *Mechanics of composite materials*, Taylor & Francis, Inc., Levittown, PA.
Kharouf, N., McClure, G., and Smith, I. (2003). "Elasto-plastic modeling of wood bolted connections." *Comput. Struct.*, 81(8–11), 747–754.
Kim, N.-H. (2015). *Introduction to nonlinear finite element analysis*, Springer, New York.
Lee, A. W. C., Xuesong, B., and Perry, N. P. (1994). "Selected physical and mechanical properties of giant timber bamboo grown in South Carolina." *For. Prod. J.*, 44(9), 40–46.
Lekhnitskiĭ, S. G. (1968). *Anisotropic plates*, Gordon and Breach, New York.
Mahdavi, M., Clouston, P. L., and Arwade, S. R. (2011). "Development of laminated bamboo lumber: Review of processing, performance, and economical considerations." *J. Mater. Civ. Eng.*, 10.1061/(ASCE)MT.1943-5533.0000253, 1036–1042.
Oudjene, M., and Khelifa, M. (2009). "Elasto-plastic constitutive law for wood behavior under compressive loading." *Constr. Build. Mater.*, 23(11), 3359–3366.
Patton-Mallory, M., Cramer, S. M., Smith, F. W., and Pelican, P. J. (1997). "Nonlinear material models for analysis of bolted wood connections." *J. Struct. Eng.*, 10.1061/(ASCE)0733-9445(1997)123:8(1063), 1063–1070.
Ramirez, F., Correal, J., Yamin, L., Atoche, J., and Piscal, C. (2012). "Dowel-bearing strength behavior of glued laminated Guadua bamboo." *J. Mater. Civ. Eng.*, 10.1061/(ASCE)MT.1943-5533.0000515, 1378–1387.
Reynolds, T. P., Sharma, B., Harries, K., and Ramage, M. (2016). "Dowelled structural connections in laminated bamboo and timber." *Composites Part B: Eng.*, 90, 232–240.
Santos, C. L., de Jesus, A., Morais, J., and Lousada, J. (2010). "A comparison between the EN 383 and ASTM D5764 test methods for dowel-bearing strength assessment of wood: Experimental and numerical investigations." *Strain*, 46(2), 159–174.
Soltis, L. A. (1991). "European yield model for wood connections." *Proc., Structures Congress '91*, ASCE, New York, 60–63.
Yang, R. Z., Lam, F., and Xiao, Y. (2014). "Failure analysis of typical glubam with bidirectional fibers by off-axis." *Constr. Build. Mater.*, 58, 9–15.
Yu, Y., Tian, G., Wang, H., Fei, B., and Wang, G. (2011). "Mechanical characterization of single bamboo fibers with nanoindentation and microtensile technique." *Holzforschung*, 65(1), 113–119.